Multicomponent gauge cell method

Aleksey Vishnyakov and Alexander V. Neimark[a)]
Department of Chemical and Biochemical Engineering, Rutgers, The State University of New Jersey, 98 Brett Road, Piscataway, New Jersey 08854-8058, USA

(Received 30 December 2008; accepted 2 April 2009; published online 9 June 2009)

The gauge cell Monte Carlo method [Neimark and Vishnyakov, J. Chem. Phys. **122**, 234108 (2005)] for calculations of chemical potential in dense and strongly inhomogeneous fluids is extended to multicomponent systems. The system of interest is simulated in a sample cell that is placed in chemical contact with several gauge cells of limited capacity, one gauge cell per component. Thus, each component can be exchanged between the sample cell and the respective gauge cell. The sample and gauge cells are immersed into the thermal bath of a given temperature. The size of the gauge cell controls the level of concentration fluctuations for the respective component in the sample cell. The chemical potentials are rigorously calculated from the equilibrium distribution of particles between the system and the gauges, and the results do not depend on the gauge size. For large systems, the chemical potentials can be accurately estimated from the average densities in the gauge cells. The proposed method was tested against the literature data on the vapor-liquid equilibrium in a binary mixture of subcritical and supercritical fluids and against the grand canonical and Widom insertion Monte Carlo methods for a binary mixture confined to a very narrow spherical pore. The method is specifically suitable for simulations of metastable and labile states in multicomponent confined fluids. © *2009 American Institute of Physics*. [DOI: 10.1063/1.3124186]

I. INTRODUCTION

The gauge cell Monte Carlo (MC) method[1,2] is a simulation technique designed for studies of equilibria and phase transitions in confined fluids and nanostructured complex systems. In this method, the system of interest, or sample cell, is placed in chemical equilibrium at the thermostated conditions with a reservoir of particles of limited capacity called the gauge cell. The gauge cell serves as a meter for measuring the chemical potential, while its limited capacity restricts the density fluctuations that allows one to study metastable and labile states. This simulation set-up is intermediate between the canonical ensemble (CE) and grand canonical ensemble (GCE) and corresponds to the mesoscopic canonical ensemble (MCE).[2] Since its introduction in 2000,[1] the gauge cell method found various applications, including adsorption and capillary condensation of Lennard-Jones (LJ) fluid on nanoporous materials with cylindrical,[3] spherical,[4] and ink-bottle pores,[5] water on carbons,[6] and linear and branched alkanes in carbon nanotubes,[7–9] formation of liquid bridges/junctions in nanocapillaries,[10] bubble cavitation in stretched metastable liquid,[11] nucleation of droplets,[12,13] adsorption deformation,[14] and segregation in surfactants.[15] The original gauge cell method,[1] in which the chemical potential is measured based on the mean density in the gauge cell, was extended to extremely small confinements with the ideal gas gauge cell (IGGC) method.[2] The other extensions of the method include its coupling with Widom insertions[6] and configurational bias,[7,8] as well as various simplifications of the computational schemes.[9]

In this work, the gauge cell method is extended to multicomponent systems. To measure chemical potentials in M-component system we introduce M gauge cells, one per component. The gauge cells may have different capacities that allow one to control the density fluctuations of individual components within different margins. Moreover, some of the components may be kept in equilibrium with infinite reservoirs of respective particles which leads to hybrid grand canonical and mesocanonical conditions. The method is described in Sec. II. In Secs. III and IV, we present two case studies: a bulk binary mixture of subcritical and supercritical components and a binary LJ fluid under an extreme confinement. In Sec. IV, we present a critical discussion of the advantages of the proposed method compared to other MC simulation schemes suggested for calculating chemical potentials in multicomponent systems.

II. GAUGE CELL METHOD FOR MULTICOMPONENT SYSTEMS

Let us consider a thermostated M-component system confined to a volume V subjected to external potential fields. Our goal is to determine the chemical potentials of individual components $\mu_1,\ldots,\mu_M$ at a given mixture composition $N_1,\ldots,N_M$ (N_i is the number of particles of component i or loading). In the multicomponent gauge cell method, we introduce M separate gauge cells for each mixture component

a)Author to whom correspondence should be addressed. Electronic mail: aneimark@rutgers.edu.

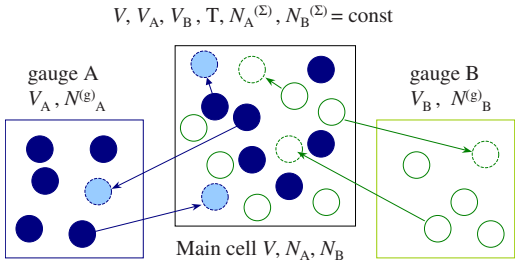

FIG. 1. (Color online) Schematics of the gauge cell simulations with two components A and B. The simulation is carried out in three cells: main cell and two implicit gauge cells for two components. MC moves include displacement in the main cell, creations/destruction of particles of each component. The volumes of all three cells, temperature, and the total numbers of particles of each component $N_X^{(\Sigma)}=N_X+N_X^{(g)}$ are constant.

(Fig. 1). Thus, the simulation is carried out in $M+1$ cells: the sample cell and M gauge cells, so that the particles of component i are exchanged with only one respective gauge cell of volume $V_i^{(g)}$. The equation of state for the gauge cell, i.e., the chemical potential as a function of the number of particles, or loading in the gauge cell $\mu_i^{(g)}(N_i^{(g)},V_i^{(g)},T)$, is assumed known. This way, the gauge cells serve as meters of the chemical potentials of the respective components located in the sample cell. The simulation is performed, similarly to the pore-fluid Gibbs ensemble MC (GEMC) scheme,[16] in a system of several cells with the exchange of particles between the cell at isothermal conditions to provide the chemical equilibrium. The total number of particles of each component is kept constant, $N_i^{(\Sigma)}=N_i+N_i^{(g)}$. The sample cell volume V and the gauge cell volumes $V_i^{(g)}$ are fixed. That is, one deals with CE of $M+1$ mechanically isolated cells.

Since the interactions between the sample cell and the gauge cells are decoupled and each gauge cell contains only one component, we restrict our further consideration to binary systems; generalization to a larger number of components is trivial. For a binary sample system of two components A and B interacting with two gauge cells, the total Helmholtz free energy is defined through the canonical partition function, which takes into account possible distributions of particles between the cells,

$$F^{(\Sigma)}(N_A^{(\Sigma)},N_B^{(\Sigma)},V,T) = -kT\ln\left\{\sum_{N_A=0}^{N_A^{(\Sigma)}}\sum_{N_B=0}^{N_B^{(\Sigma)}}\exp\left[-\frac{1}{kT}[F(N_A,N_B,V,T) + F_A^{(g)}(N_A^{(\Sigma)}-N_A,V_A^{(g)},T)+F_B^{(g)}(N_B^{(\Sigma)}-N_B,V_B^{(g)},T)]\right]\right\}. \quad (1)$$

Here, $F(N_A,N_B,V,T)$ is the Helmholtz free energy defined through the canonical partition function, which has the following form for a two-component system:

$$F(N_A,N_B,V,T) = -kT\ln Q(N_A,N_B,V,T) = kT\ln\left[\frac{1}{\Lambda_A^{3N_A}\Lambda_B^{3N_B}N_A!\,N_B!}\times\int d\mathbf{r}^N\exp(-\Phi(\mathbf{r}^N)/kT)\right], \quad (2)$$

where the total potential energy $\Phi(\mathbf{r}^N)$ is the sum of the fluid-fluid potential $\Phi_{FF}(\mathbf{r}^N)$ and the external potential $\Phi_{SF}(\mathbf{r}^N)$; $F_A^{(g)}(N_A^{(g)},V_A^{(g)},T)$ and $F_B^{(g)}(N_B^{(g)},V_B^{(g)},T)$ are the Helmholtz free energies of the gauge cells with respective number of particles, $N_A^{(g)}=N_A^{(\Sigma)}-N_A$ and $N_B^{(g)}=N_B^{(\Sigma)}-N_B$.

The canonical chemical potential μ_A^+ of component A represents the work of insertion of an additional particle of component A into the sample system and is defined as the difference of the Helmholtz free energies of the systems with N_A+1 and N_A particles, while N_B remains unchanged,

$$\mu_A(N_A,N_B) = F(N_A+1,N_B,V,T)-F(N_A,N_B,V,T) = -kT\ln\left(\frac{V}{\Lambda_A^3(N_A+1)}\right)-kT\ln\left(\frac{1}{V}\int d\mathbf{r}_{N_A+1}\times\langle\exp(-\Phi(r_{N_A+1},\mathbf{r}^{N_A},\mathbf{r}^{N_B})/kT)\rangle_{N_A,N_B}\right), \quad (3)$$

where $\Phi(\mathbf{r}_{N_A+1},\mathbf{r}^{N_A},\mathbf{r}^{N_B})$ accounts for interactions of (N_A+1)th particle located at $\mathbf{r}_{N_A+1}$ with N_A particles of component A and N_B particles of component B as a function of their positions $\mathbf{r}^{N_A}$, $\mathbf{r}^{N_B}$ and external potential Φ_{SF}.

Equation (3) defines the chemical potential as a discrete function of (N_A,N_B) through the finite differences of the Helmholtz free energy. Provided the integration in Eq. (3) is carried out over the entire configuration space, $\mu_A^+(N_A,N_B)$ and $\mu_B^+(N_A,N_B)$ are single-valued functions of the number of particles of each component in the system. The inverse functions, loadings versus chemical potentials, represent the isotherms for a given system, which may be expressed as either $N_A(\mu_A^+,N_B)$, $N_B(\mu_B^+,N_A)$, or $N_A(\mu_A^+,\mu_B^+),N_B(\mu_A^+,\mu_B^+)$.

The probability to observe a configuration of (N_A,N_B) particles in the main cell and, respectively, $(N_A^{(g)},N_B^{(g)})$ particles in the gauge cells is proportional to

$$P(N_A,N_B) = P(N_A^{(g)},N_B^{(g)}) \propto \exp\left\{-\frac{1}{kT}[F(N_A,N_B,V,T) + F_A^{(g)}(N_A^{(g)},V_A^{(g)},T)+F_B^{(g)}(N_B^{(g)},V_B^{(g)},T)]\right\} \quad (4)$$

and

$$P(N_A+1,N_B) = P(N_A^{(g)}-1,N_B^{(g)}) \propto \exp\left\{-\frac{1}{kT}[F(N_A+1,N_B,V,T)+F_A^{(g)}(N_A^{(g)}-1,V_A^{(g)},T)+F_B^{(g)}(N_B^{(g)},V_B^{(g)},T)]\right\}, \quad (5)$$

respectively. Thus, the canonical chemical potentials μ_A^+,μ_B^+ of the series of (N_A,N_B,V,T) states sampled in the gauge

cell simulation are determined from the ratios of the sampling probabilities. Combining Eqs. (4) and (5), we obtain

$$\frac{P(N_A+1,N_B)}{P(N_A,N_B)}=\frac{P(N_A^{(g)}-1,N_B^{(g)})}{P(N_A^{(g)},N_B^{(g)})}=\exp\left\{-\frac{1}{kT}[\mu_A(N_A,N_B,V,T)-\mu_A^{(g)}(N_A^{(g)}-1,V_A^{(g)},T)]\right\}, \tag{6}$$

and, correspondingly,

$$\mu_A(N_A,N_B,V,T)=\mu_A^{(g)}(N_A^{(g)}-1,V_A,T)+kT\ln(P(N_A^{(g)},N_B^{(g)})/P(N_A^{(g)}-1,N_B^{(g)})), \tag{7}$$

where $\mu_A^{(g)}(N_A^{(g)}-1,V_A^{(g)},T)=F_A^{(g)}(N_A^{(g)},V_A^{(g)},T)-F_A^{(g)}(N_A^{(g)}-1,V_A^{(g)},T)$ is the chemical potential of $N_A^{(g)}-1$ particles in the gauge cell.

Equation (7) constitutes the foundation for computing the canonical isotherm of the main cell in the form of $\mu_{A|B}(N_A,N_B)$ from the probability distributions of the number of particles in the gauge cells $P(N_A^{(g)},N_B^{(g)})$. Since in the derivation of Eq. (7) no assumptions or approximations were made, the result depends neither on the sizes of the gauge cells nor on the total numbers of particles $N_{A|B}^{(\Sigma)}=N_{A|B}+N_{A|B}^{(g)}$ in a given simulation. To construct the canonical isotherm in a wide range of N_A and N_B, one has to perform the gauge cell simulations varying the total number of particles in the system and/or the size of the gauge cells. In so doing, from one simulation at given $N_A^{(\Sigma)}$, $N_B^{(\Sigma)}$, $V_A^{(g)}$, and $V_B^{(g)}$, several points of the isotherm can be computed around the most probable loading $(\hat{N}_A,\hat{N}_B)$ with precision of one particle.

The equations derived above do not imply any restrictions on the gauge cells and on the interactions of particles within the gauge cells. The equation of the gauge fluid can be chosen for reasons of convenience. The most practical and theoretically sound choice is to consider particles in the gauge cell as ideal.[2] In this case, the chemical potential at loading $N_{A|B}^{(g)}$ in the gauge cell equals

$$\mu_{IG}(N_{A|B}^{(g)})=-kT\ln\left(\frac{V_{A|B}^{(g)}}{\Lambda_{A|B}^3(N_{A|B}^{(g)}+1)}\right), \tag{8}$$

and Eq. (7) reduces to

$$\mu_A(N_A,N_B,V,T)=-kT\ln\left(\frac{V_A^{(g)}}{\Lambda_A^3 N_A^{(g)}}\right)+kT\ln(P(N_A^{(g)},N_B^{(g)})/P(N_A^{(g)}-1,N_B^{(g)})). \tag{9}$$

At sufficiently large loadings $N\gg 1$, the most probable loadings equal the average loadings, $\hat{N}_{A|B}=\bar{N}_{A|B}$, and the standard condition of equality of the chemical potentials applies

$$\mu_{A|B}=(\partial F/\partial N_{A|B})_{N_{B/A}V,T}=\mu_{A/B}^{(g)}=(\partial F_{A|B}^{(g)}/\partial N_{A|B}^{(g)})_{V_{A|B}^{(g)},T}. \tag{10}$$

Therefore,

$$\mu_{A|B}(\bar{N}_A,\bar{N}_B,V,T)=-kT\ln\left(\frac{V_{A|B}^{(g)}}{\Lambda_{A|B}^3(\bar{N}_{A|B}^{(g)}+1)}\right). \tag{11}$$

Equation (11) constitutes the foundation of the mean density gauge cell (MDGC) method. The computational scheme of the IGGC method corresponds to MCE,[2] which is intermediate between CE and GCE. In GCE, the system under study is open for the exchange of particles with the unlimited reservoir of ideal particles, so that the fluctuations of N are unconstrained. In CE, the system is closed and N_A and N_B are constant. In MCE, the system under study is semiopen: it exchanges particles with the finite volume reservoirs of ideal particles (gauge cells of volumes $V_{A|B}$). Thus, the system mass fluctuates and the level of fluctuations is controlled by the reservoir volumes. This is the key property of MCE. As $V_{A|B}^{(g)}$ increases to infinity, MCE transforms into GCE. As $V_{A|B}$ diminishes, MCE reduces to CE. Since the volumes of the reservoirs of different components are independent from each other, it is possible to maintain different levels of density fluctuations for different components.

The simulation procedure in the IGGC method is as follows. Three types of MC moves are performed: particle displacement within the sample cell, particle insertion into the sample cell from the gauge cell of the respective component, and particle removal from the sample cell to the gauge cell of the respective component. It is possible to introduce additional moves to help establish equilibrium in the sample cell faster: swap of particles of different identity in the sample cell and change in the particle identity $(A\rightarrow B)$ in sample cell combined with particle insertion into the B-gauge cell and particle removal from the A-gauge cell. These additional moves were not implemented in the examples presented in this work. The displacement step in the sample cell is identical to that in CE: the trial move is accepted with the probability

$$p_{dis}=\min\{1,\exp[-\Delta E/kT]\}, \tag{12}$$

where ΔE is the change of the configuration energy upon displacement. The trial insertion into the sample cell from the gauge cell is accepted with the probability

$$p_{ins}=\min\{1,\exp[-\Delta E/kT+\ln(V_{A|B}^{(g)}(N_{A|B}+1)/VN_{A|B}^{(g)})]\}, \tag{13}$$

and the trial removal from the sample cell into the gauge cell is accepted with the probability

$$p_{rem}=\min\{1,\exp[-\Delta E/kT+\ln(V(N_{A|B}^{(g)}+1)/V_{A|B}^{g}N_{A|B})]\}. \tag{14}$$

The acceptance probabilities [Eqs. (12)–(14)] provide the fulfillment of the MCE particle distribution between the main and gauge cells,

TABLE I. Conditions and results of simulations of binary LJ system representing methane-pentane mixture at $T=444.26$ K and $P=6.87$ MPa.

Composition, x_B	Density $\rho\sigma_B^3$			System size			
	Total	Methane	Pentane	δ_{AB}	L/σ_B	$N_A^{(\Sigma)}$	$N_B^{(\Sigma\Sigma}$
0	0.2025		0.2029	0.0	14.0		
0.0085	0.2025	0.0018	0.2012	0.0	14.0	583	5
0.1	0.199	0.0199	0.1789	−0.09	15.0	634	97
0.2	0.177	0.0354	0.1416	−0.01	16.0	610	175
0.25	0.151	0.0377	0.1131	−0.02	17.0	586	215
0.34	0.115	0.0391	0.0759	0.025	18.0	473	258
0.4	0.099	0.0396	0.0593	0.01	19.0	437	302
0.5	0.082	0.0410	0.0410	0.005	20.0	358	358
0.6	0.072	0.0432	0.0288	0.004	21.0	297	430
0.7	0.067	0.0469	0.0201	0.001	21.0	216	464
0.8	0.063	0.0504	0.0126	0.0	22.0	164	567
0.9	0.059	0.0531	0.0059	0.0	23.0	102	676
0.992	0.059 05	0.0586	0.000 47	0.0	22.0	5	654
1	0.059 05	0.059 05		0.0	22.0	0	659

$$P_{N_A,N_B} = P_{N_A^{(g)},N_B^{(g)}} \propto \frac{\Lambda_A^{N_A^{(g)}} \Lambda_B^{N_B^{(g)}} N_A^{(g)}!\, N_B^{(g)}!}{(V_A^g)^{N_A^{(g)}} (V_B^g)^{N_B^{(g)}}} \times \exp\left\{ -\frac{1}{kT}[F(N_A,N_B,V,T)] \right\}. \quad (15)$$

The number of insertion and removal attempts must be equal for each component. In this work, one insertion and one removal steps were attempted per each trial displacement.

III. BINARY MIXTURE OF SUBCRITICAL AND SUPERCRITICAL COMPONENTS, MDGC METHOD

For bulk homogeneous fluids, the MDGC technique has the same applications, as the Widom insertion method: calculation of chemical potentials at fixed densities and compositions, but somewhat better efficiency.[2] We tested the MDGC method against the literature data of Wilson and Lee[17] on a binary LJ mixture of subcritical and supercritical components. The components represented methane and pentane at $T=444.26$ K and $P=6.87$ MPa. At these conditions, pure pentane is a liquid ($T_c^{(A)}=469.7$ K) and pure methane is a supercritical fluid ($T_c^{(B)}=190$ K). (From now on, we shall use A index for LJ pentane and B index for LJ methane.) Vapor-liquid equilibrium in the pentane-methane mixture at this condition corresponds to methane molar fractions of $x_B^{(vap)}=0.3364$ and $x_B^{(liq)}=0.2569$.[17] LJ parameters of $\sigma_A=0.5282$ nm and $\varepsilon_A/k=350$ K and $\sigma_B=0.374$ nm and $\varepsilon_B/k=190$ K were used for pentane and methane, respectively. These parameters were fitted to experimental data for pure systems.[17]

Because pentane is by no means a LJ fluid, the LJ model with fixed energetic parameters does not reproduce the experimental binary vapor-liquid phase diagram: at a given temperature, pressure, and the liquid composition (x_A,x_B), the composition of the equilibrium vapor (y_A,y_B) deviates from the experimental value. In order to achieve a good agreement with the experiment, Wilson and Lee[17] introduced a composition-dependent adjustable parameter δ_{AB} for interactions between LJ methane and pentane particles: $\varepsilon_{AB}=(1+\delta_{AB}(x_A))\sqrt{\varepsilon_B\varepsilon_A}$. We varied δ_{AB} with the composition according to this prescription; the values of δ_{AB} are given in Table I. The simulation system contained from 570 to 670 LJ particles. The length of each simulation was 1×10^8 steps (including insertions, destruction, and displacements), first 3×10^7 steps were discarded. During the equilibration, the sizes of the gauge cells were automatically adjusted to accommodate 30 particles each in average, and the maximum displacement distance was adjusted to keep the acceptance ratio between 40% and 60%.

In such large system, it is safe to employ the MDGC method and calculate the chemical potentials $\mu_{A/B}$ from the mean densities in the gauge cells, Eq. (11). For each composition x, we determined the excess chemical potentials $\mu_{ex}=\mu-RT\ln(\rho\Lambda^3)$ for both components. The results shown in Fig. 2 agree perfectly with those of Wilson and Lee[17] with the exception of pentane-rich region (>85% mol). The end points of the calculated isotherm correspond to the pure components, which chemical potentials are in excellent agreement with the LJ fluid equation of state,[18] while some dis-

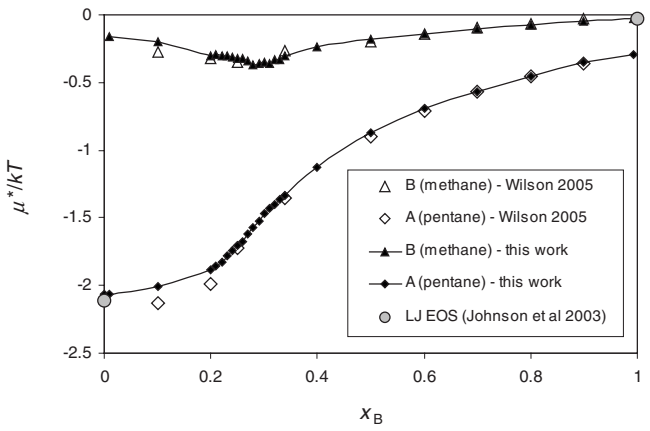

FIG. 2. Excess chemical potentials in binary LJ system representing methane—pentane binary mixture at $T=444$ K and $P=6.87$ MPa.

crepancies between the results obtained in Ref. 17 and the LJ equation of state are found when the pure component limit is approached (Fig. 2).

IV. BINARY LJ MIXTURE IN AN EXTREME CONFINEMENT, IGGC METHOD

Let us consider sorption of a binary LJ mixture in an extremely narrow spherical pore of two molecular diameters in radius which corresponds to internal diameter $D_{in}=D-\sigma_{sf}$ of 1.17 nm. This confinement was used in our earlier work[2] as a case study example for the single component IGGC method. The LJ parameters of both components ($\varepsilon/k=101.5$ K, $\sigma=0.3615$ nm, $r_{cutoff}=5\sigma$) were equal. This LJ fluid effectively models nitrogen at 77.4 K.[19] The adjustable energy parameter δ_{AB} was set to -0.25, so the interaction between the unlike particles was 25% weaker than those between two identical particles. The solid wall was modeled as a uniform layer of "smeared out" LJ atoms which produces the solid-fluid potential

$$U_{sf}^{(sph)}(r,R) = 2\pi\rho_s\varepsilon_{sf}\sigma_{sf}^2\left[\frac{2}{5}\sum_{i=0}^{9}\left(\frac{\sigma_{sf}^{10}}{R^i r^{10-i}}+(-1)^i\frac{\sigma_{sf}^{10}}{R^i(r-2R)^{10-i}}\right)-\sum_{i=0}^{9}\left(\frac{\sigma_{sf}^{4}}{R^i r^{4-i}}+(-1)^i\frac{\sigma_{sf}^{4}}{R^i(r-2R)^{4-i}}\right)\right]. \quad (16)$$

In Eq. (16), r is the radial coordinate of the fluid particle reckoned from the pore center, R is the pore radius, ρ_s is the surface number density of the adsorption centers, and ε_{sf} and σ_{sf} are the effective LJ parameters of the intermolecular solid-fluid interaction. At infinite r the potential (16) reduces to the 10-4 potential for a planar surface of LJ particles.[20] We employed the LJ parameters of the potential $\sigma_{sf}=0.3494$ nm and $\varepsilon_{sf}/k=53.22$ K and $\rho_s=15.3$ nm^{-2} for component A. These parameters were found from the best fit of the calculated nitrogen adsorption isotherm on the flat surface to the experimental isotherm on nonporous silica.[21,22] We tried two sets of solid-fluid parameters for component B: system 1 with $\varepsilon_B^{(sf)}/k=39.9$ K (component B interacts with the wall 25% weaker than for component A) and system 2 with $\varepsilon_B^{(sf)}/k=47.9$ (component B interacts with the wall 10% weaker than for component A). The temperature was $kT/\varepsilon_{ff}=0.762$, which corresponds to the nitrogen normal boiling temperature of 77.4 K. The solid-fluid potentials are given in Fig. 3.

The pore under consideration can accommodate at most 16 particles. In such small system the IGGC method is required for better accuracy. In our simulations, the gauge volumes were automatically adjusted during the equilibration period so that $\hat{N}_A^{(g)}=\hat{N}_B^{(g)}=6$ In Fig. 4(a), we present a typical example of the results of a single IGGC simulation with the

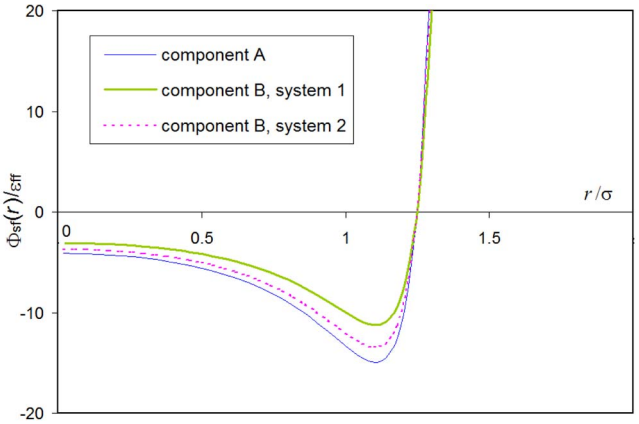

FIG. 3. (Color online) Solid-fluid potential for the particles of both components in the narrow spherical pore. In system 1, the contrast between sorption potentials for the two components is very large (25%), which equals to $2\varepsilon_{FF}$ for a particle located near the wall. In system 2, the contrast is smaller (10%).

fixed total numbers of particles of each component, $N_{A|B}^{(\Sigma)}=N_{A|B}+N_{A|B}^{(g)}$. Each simulation yields a two-dimensional (2D) array of the probabilities $P(N_A,N_B)$ to observe a particular composition in the sample cell (N_A,N_B). The chemical potentials $\mu_{A|B}(N_A,N_B)$ are calculated from this set of data using Eq. (9). Figure 4(b) shows the chemical potential of component A as a 2D function of loadings N_A and N_B calculated from the probability data presented in Fig. 4(a). The statistical errors are smallest close to the most probable configuration and become very high toward the periphery of the distribution, since these configurations are observed insufficiently frequently. To build a complete isotherm for such a small system with precision of one particle, one has to perform several overlapping simulations by varying the total number of particles in the simulation system. The resulting adsorption isotherms composed from the data points obtained in a series of simulations with different $N_A^{(\Sigma)}$ and $N_B^{(\Sigma)}$ are presented in Fig. 4(c) in the form of the equilibrium loading of component B, $N_B(\mu_B,N_A)$ as the function of the chemical potential μ_B of component B at a fixed loading of component N_A for $N_A=0$ (single component adsorption), $N_A=3$, and $N_A=6$ (correspondingly, $N_A^{(\Sigma)}=9$, $N_B^{(\Sigma)}=12$). The chemical potentials calculated in IGGC simulations with the different total number of particles practically coincide. This confirms that the proposed simulation scheme is consistent and the results do not depend on the gauge cell size and the total number of particles employed. The same figure shows the selected results from the Widom particle insertion method.[23] The agreement is excellent with the exception of very dense packings, where the efficiency of Widom insertions is hindered.

The corner point ($N_A=N_B=0$) in Figs. 4(a) and 4(b) corresponds to the empty pore. The respective chemical potential $\mu_{A|B}^{+}(0,0)$ is defined as the work of insertion of the first particle in the empty pore. For component B, $\mu_B^{+}(0,0)$ corresponds to the first point on the isotherm $N_B(\mu_B,0)$ in Fig. 4(c) at $N_B=0$; it is determined by the pore volume and solid-potential $\Phi_{SF}(\mathbf{r}^N)$,

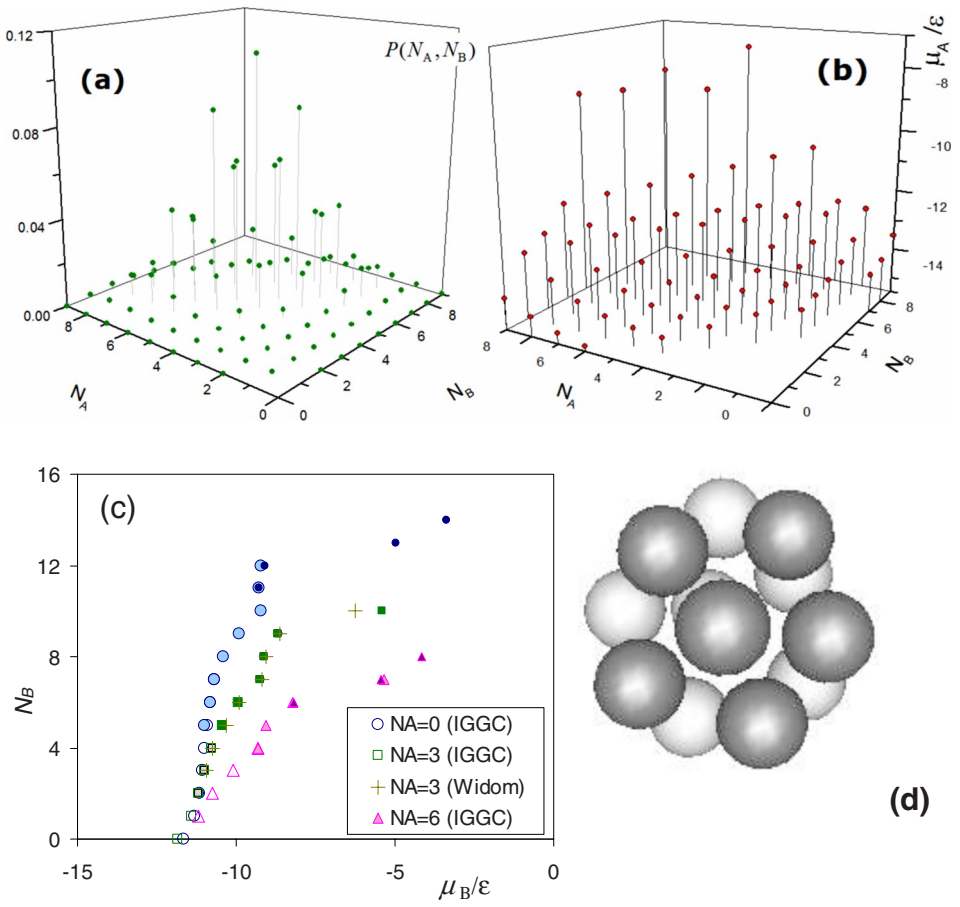

FIG. 4. (Color online) Illustration of the IGGC simulation of the binary fluid confined to the spherical pore. (a) Example of the probability histogram $P(N_A,N_B)$ obtained in a single IGGC simulation with $N_B^{(\Sigma)}=N_A^{(\Sigma)}=12$ and $\hat{N}_B=\hat{N}_A=6$. (b) Canonical chemical potential μ_A of component A as a function of loadings N_A and N_B obtained from the series of IGGC simulations. (c) Adsorption isotherms of component B presenting the equilibrium loading N_B as the function of the chemical potential μ_B of component B at fixed loadings of component N_A for $N_A=0$ (single component adsorption, circles), $N_A=3$ (squares), and $N_A=6$ (triangles). Different colors correspond to different total numbers of molecules $N^{(\Sigma)}=N_B^{(\Sigma)}+N_A^{(\Sigma)}$ in the system: $N^{(\Sigma)}=10$ (open symbols), $N^{(\Sigma)}=14$ (gray symbols), and $N^{(\Sigma)}=18$ (closed symbols). The results do not depend on the total number of molecules in the system. $\hat{N}_B^{(g)}=\hat{N}_A^{(g)}=6$. (d) Typical molecular configuration of the binary fluid in the pore at $N_B+N_A=12$.

$$\mu_B^+(0,0) = -kT\ln\left(\frac{V}{\Lambda_B^3}\right) - kT\ln\left(\frac{1}{V}\int \exp(-\Phi_{SF,B}(\mathbf{r})/kT)d\mathbf{r}\right),$$
$$= -kT\ln\left(\frac{V_B^{(g)}}{\Lambda_B^3 N_B^{(\Sigma)}}\right) + kT\ln\frac{(P(N_B^{(g)}=N_B^{(\Sigma)},N_A^{(g)}=N_A^{(\Sigma)})}{P(N_B^{(g)}=N_B^{(\Sigma)}-1,N_A^{(g)}=N_A^{(\Sigma)})}. \quad (17)$$

Note that Eq. (17) holds for any IGGC simulation disregarding the total number of particles $N_A^{(\Sigma)}$ and $N_B^{(\Sigma)}$ employed; however the reliable estimates can be made from simulations with small number of particles when probably all particles that congregate in the gauge cells are sufficiently large. The first points on the isotherms $N_B(\mu_B,3)$ and $N_B(\mu_B,6)$ at $N_B=0$ correspond to the works of insertion of particle B in the pore containing, respectively, three and six particles of component A. They are defined as $\mu_B^+(0,3)$ and $\mu_B^+(0,6)$.

In such an extreme confinement, sorption is governed by an interplay of the solid-fluid interactions and the steric effects. The more strongly adsorbing component A wins the competition for the pore space at the same chemical potentials, especially at lower ε_{sf} for B. At higher loadings, the chemical potential is mainly determined by the total number of particles located in the pore rather than by composition, as steric effects prevail over the fluid-fluid energy dependence on the composition [Fig. 4(b)]. However, the role of fluid-fluid interactions remains substantial. For example, in the case of pure component B ($N_A=0$), the chemical potential is almost equal for $N_B=10$, 11, and 12, so the isotherm $N_B(\mu_B,0)$ exhibits a step [Fig. 4(c)]. This effect was described in Ref. 2 as a transition from disordered ten particle configurations to ordered 12 particle configurations, in which particles form a compact shell at the wall with a near-perfect fivefold symmetry. Since the unlike fluid-fluid interactions are unfavorable, such close-packed configurations, composed of equal numbers of particles of components A and, B experience a visible segregation shown in Fig. 4(d). Integration of the isotherms given in Fig. 4(c) gives the free energies of different configurations and can be used for analyses of stability of the states of total equal and different compositions. If we look for instance at the three states with 12 particles on the isotherms given in Fig. 4(c), ($N_A=0,N_B=12$), (N_A

$=3, N_B=9$), and ($N_A=N_B=6$), the highest chemical potential of component B corresponds to the symmetric segregated state.

In confinements so narrow, CE isotherms are distinct from GCE isotherms. However, GCE isotherm can be reconstructed from the CE isotherm that provides an additional test of the consistency of simulations performed in different ensembles. The probability to observe (N_A, N_B) composition in GCE at given chemical potentials (μ_A, μ_B) is determined by the Helmholtz free energy F, which can be calculated from the CE isotherm as

$$F(N_A,N_B,V,T) = \sum_{i=0}^{N_A-1} \mu_A^+(i,0,V,T) + \sum_{i=0}^{N_B-1} \mu_A^+(N_A,i,V,T) = \sum_{i=0}^{N_B-1} \mu_A^+(0,i,V,T) + \sum_{i=0}^{N_A-1} \mu_A^+(i,N_B,V,T). \tag{18}$$

Note that any order of addition of the particles of different components may be employed in Eq. (18). The loading computed in the grand canonical MC (GCMC) simulation as a function of the chemical potential is the GCE average

$$N_A^{(GCE)}(\mu_A,\mu_B) = \sum_{N_A=0}^{\infty} \sum_{N_B=0}^{\infty} N_B \exp(\mu_A N_A + \mu_B N_B - F(N,V,T))/\Xi(\mu,V,T), \tag{19}$$

where $\Xi(\mu,V,T)$ is the grand canonical partition function,

$$\Xi(\mu,V,T) = \sum_{N=0}^{\infty} \exp(-\beta(F(N,V,T) - \mu N)). \tag{20}$$

The comparison of the GCE isotherms recalculated from the data obtained with the IGGC method with the GCMC results is shown in Fig. 5. We calculated the GCE adsorption isotherms from the bulk fluid of constant composition $x_B=0.9$ by varying the bulk pressure from a very low pressure of about $10^{-5}-10$ atm for systems 1 and 2 with weaker and stronger solid-fluid attraction of component B. The GCE adsorption isotherms of components A and B are given in Fig. 5(a), and the selectivity to component B $S_i=(1-y_B)x_B/(1-x_B)y_B$ (in this equation, x_B is the molar fraction of component B in the pore, y_B is its fraction in the equilibrium vapor) is given in Fig. 5(b). The adsorption behaviors in systems 1 and 2 are qualitatively different: selectivity increases with pressure in system 1 and decreases in system 2. In system 1, the minimum of the solid-fluid potential for component A is $4kT$ lower than for the component B, and the pore is strongly selective to component A. The density of component A in the pore is much larger than that of component B despite that B prevails in the bulk. As the pressure builds up and fluid-fluid interactions become more important, selectivity to B even decreases (and selectivity to component B, respectively, increases) because the interactions between the particles of different components are unfavorable. In system 2, the prevalence of component B in the bulk mixture does not outweigh the difference in the solid-fluid energy also; however, being close to 0.1 at low pressures, S_B slowly increases as the pressure builds up.

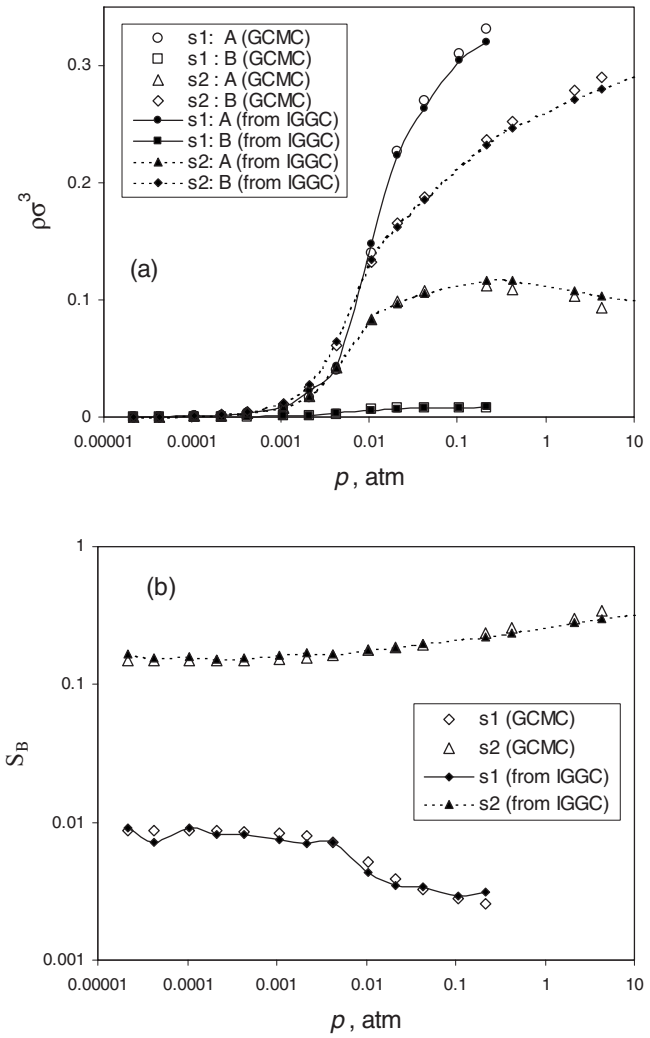

FIG. 5. Adsorption from the bulk binary mixture of fixed composition $x_B=0.9$: (a) partial adsorption isotherms (b) and selectivity to component B as functions of the bulk pressure. For both systems 1 and 2, the isotherms obtained in direct GCMC simulations agree well with the isotherms reconstructed via Eqs. (18)–(20) from the CE isotherms obtained using the binary IGGC method.

As seen from Fig. 5, the GCE isotherms reconstructed from the CE isotherms obtained in the IGGC method excellently coincide with the GCMC isotherm. Although the statistical fluctuations are much stronger for the reconstructed isotherms, an overall agreement for both the partial densities and selectivity is satisfactory.

V. DISCUSSION AND CONCLUSION

We extended the gauge cell MC simulation method to multicomponent systems and tested it against the literature data and the results of other well-established simulation techniques. The proposed method can be summarized as follows. The system of interest is simulated in a sample cell that is placed in chemical contact with several gauge cells of limited capacity, one gauge cell per component. Thus, each component can be exchanged between the sample cell and the respective gauge cell. The sample and gauge cells are immersed into the thermal bath of a given temperature. The size of the gauge cell controls the level of concentration fluctuations for the respective component in the sample cell. This

scheme allows one to (1) obtain CE chemical potentials of all components in the system and (2) control concentration fluctuations for each component that is required for simulations of metastable and labile states. We developed two versions of the multicomponent gauge cell method: the ideal gas gauge (IGGC) method and the mean density (MDGC) method. The IGGC method is based on a rigorous statistical-mechanical treatment of the sample system in the mesocanonical ensemble. In IGGC method, the chemical potentials are calculated from the histograms of probabilities of equilibrium particle distribution between the sample and gauge cells. This method allows one to determine the chemical potential with the precision of one molecule that has an advantage for modeling confined systems comprised of small number of particles. A shortcoming of the IGGC method is the necessity to calculate multidimensional probability histograms that may become inefficient and impractical in relatively large multicomponent systems. The MDGC method represents a simplified version, where the chemical potentials are calculated from the average densities in the respective gauge cells. This technique is designed for relatively large systems, where the free energy may be considered as a continuous function of the number of particles.

We tested the proposed method against the literature data and the results of other well-established techniques. The MDGC method was applied to study the vapor-liquid equilibrium in a binary mixture of subcritical pentane and supercritical methane modeled as LJ fluids with adjustable energetic parameters according to the prescription of Wilson and Lee.[17] The results obtained agree with those presented in Ref. 17. The IGGC method was applied to study the equilibrium distribution in a binary mixture of LJ particles adsorbed within a spherical pore that can accommodate at most 16 particles. The IGGC simulation results were found consistent with the results of the GCMC[24] and Widom insertion methods. The IGGC is most efficient for dense inhomogeneous mixtures exhibiting segregation of components when the Widom method is impractical.

As of now, free energies of multicomponent systems as well as the phase equilibria were studied using Widom insertion technique,[25,26] thermodynamic integration of GCMC adsorption isotherms[27] and Gibbs–Duhem integration,[28–32] GEMC (e.g., Refs. 33–36), umbrella sampling,[37–39] histogram reweighting,[40–44] and, recently, Wang–Landau technique.[45–47] Popular approaches to polymer solutions include the osmotic ensemble,[48] where the number of polymeric molecules is fixed (for their insertions and removals being extremely inefficient), while small molecules are considered at fixed chemical potentials and may be exchanged between the main system and an infinite bulk reservoir, as in GCMC, and the volume fluctuates at a fixed pressure. Another approach to the simulations of polymeric mixtures involves pseudoensembles, where the grand canonical conditions are emulated using volume change MC steps.[48] Each of these techniques has certain pros and cons (see, e.g., Ref. 49). We see the main advantage of our method in possibility to control the density fluctuations separately for each component, which makes the gauge cell method especially suitable for the simulations of thermodynamically metastable and labile systems, which are often inaccessible in the grand canonical and osmotic ensembles. Since there are no restrictions on the gauge cell sizes, the method enables "hybrid" simulations, where one component is kept at constant chemical potential (which may be achieved using an unlimited gauge cell for this component), while the loadings of other components fluctuate within controlled margins. The gauge cell method also holds a certain advantage over the umbrella sampling, histogram reweighting, and multicanonical[50,51] schemes since it samples a trajectory of configurations, which are stabilized at certain conditions. By controlling the density fluctuations, the method enables the focused sampling of configurations around a certain labile state, such as a nucleus, that leads to a desired statistics of the transient states, which are rarely observed in the unconstrained sampling. This is specifically important in studies of multicomponent nucleation. An example of application of the gauge cell method for multicomponent nucleation will be published elsewhere. It is worth noting that the proposed method with various hybrid simulation setups can be used for measuring the solubilities of chemicals in complex systems when the "system" is treated at the canonical or grand canonical conditions and the dissolved species—at the mesocanonical conditions, which restrict their density fluctuations according to the volumes of the respective gauge cells.

[1] A. V. Neimark and A. Vishnyakov, Phys. Rev. E **62**, 4611 (2000).
[2] A. V. Neimark and A. Vishnyakov, J. Chem. Phys. **122**, 234108 (2005).
[3] A. Vishnyakov and A. V. Neimark, J. Phys. Chem. B **105**, 7009 (2001).
[4] A. V. Neimark and A. Vishnyakov, J. Phys. Chem. B **110**, 9403 (2006).
[5] A. Vishnyakov and A. V. Neimark, Langmuir **19**, 3240 (2003).
[6] M. Jorge and N. A. Seaton, Mol. Phys. **100**, 3803 (2002).
[7] J. W. Jiang, S. I. Sandler, and B. Smit, Nano Lett. **4**, 241 (2004).
[8] J. W. Jiang and S. I. Sandler, Langmuir **22**, 7391 (2006).
[9] J. P. B. Mota and I. Esteves, Adsorption **13**, 21 (2007).
[10] A. Vishnyakov and A. V. Neimark, J. Chem. Phys. **119**, 9755 (2003).
[11] A. V. Neimark and A. Vishnyakov, J. Chem. Phys. **122**, 054707 (2005).
[12] A. V. Neimark and A. Vishnyakov, J. Phys. Chem. B **109**, 5962 (2005).
[13] A. V. Neimark and A. Vishnyakov, J. Chem. Phys. **122**, 174508 (2005).
[14] P. Kowalczyk, A. Ciach, and A. V. Neimark, Langmuir **24**, 6603 (2008).
[15] F. X. Zheng, X. R. Zhang, and W. C. Wang, Langmuir **24**, 4661 (2008).
[16] A. Z. Panagiotopoulos, Mol. Phys. **62**, 701 (1987).
[17] D. S. Wilson and L. L. Lee, J. Chem. Phys. **123**, 044512 (2005).
[18] J. K. Johnson, J. A. Zollweg, and K. E. Gubbins, Mol. Phys. **78**, 591 (1993).
[19] P. I. Ravikovitch, A. Vishnyakov, R. Russo, and A. V. Neimark, Langmuir **16**, 2311 (2000).
[20] W. A. Steele, *The Interactions of Gases with Solid Surfaces* (Pergamon, New York, 1974).
[21] P. I. Ravikovitch, S. C. O'Domhnaill, A. V. Neimark, F. Schuth, and K. K. Unger, Langmuir **11**, 4765 (1995).
[22] J. H. deBoer, B. G. Linsen, and T. J. Osinga, J. Catal. **4**, 643 (1965).
[23] B. Widom, J. Chem. Phys. **39**, 2808 (1963).
[24] G. E. Norman and V. S. Filinov, High Temp. **7**, 216 (1969).
[25] J. Vrabec and J. Fischer, Mol. Phys. **85**, 781 (1995).
[26] D. Boda, J. Liszi, and I. Szalai, Chem. Phys. Lett. **235**, 140 (1995).
[27] A. Vishnyakov, E. M. Piotrovskaya, and E. N. Brodskaya, Russ. J. Phys. Chem. **74**, 1500 (2000).
[28] B. C. Attwood and C. K. Hall, AIChE J. **54**, 1886 (2008).
[29] A. van 't Hof, C. J. Peters, and S. W. de Leeuw, J. Chem. Phys. **124**, 054906 (2006).
[30] J. P. B. Mota, I. Esteves, R. C. R. Rodrigues, and N. F. C. Formiga, Adsorption **11**, 319 (2005).
[31] A. Mori, B. B. Laird, Y. Kangawa, T. Ito, and A. Koukitu, Russ. J. Phys. Chem. **77**, S21 (2003).
[32] M. H. Lamm and C. K. Hall, AIChE J. **47**, 1664 (2001).
[33] L. L. Liu, X. N. Yang, and Z. J. Xu, J. Chem. Phys. **128**, 184712 (2008).
[34] M. Schmidt, A. Fortini, and M. Dijkstra, J. Phys.: Condens. Matter **16**,

S4159 (2004).
[35] I. Brovchenko, A. Geiger, and A. Oleinikova, J. Chem. Phys. **120**, 1958 (2004).
[36] W. T. Gozdz, K. E. Gubbins, and A. Z. Panagiotopoulos, Mol. Phys. **84**, 825 (1995).
[37] S. Punnathanam and P. A. Monson, J. Chem. Phys. **125**, 024508 (2006).
[38] P. Virnau, M. Muller, L. G. MacDowell, and K. Binder, J. Chem. Phys. **121**, 2169 (2004).
[39] B. Chen, J. I. Siepmann, and M. L. Klein, J. Am. Chem. Soc. **125**, 3113 (2003).
[40] J. Perez-Pellitero, P. Ungerer, G. Orkoulas, and A. D. Mackie, J. Chem. Phys. **125**, 054515 (2006).
[41] M. E. McKenzie and B. Chen, J. Phys. Chem. B **110**, 3511 (2006).
[42] V. K. Shen and J. R. Errington, J. Chem. Phys. **122**, 064508 (2005).
[43] G. Besold, J. Risbo, and O. G. Mouritsen, Comput. Mater. Sci. **15**, 311 (1999).
[44] J. J. Potoff and A. Z. Panagiotopoulos, J. Chem. Phys. **109**, 10914 (1998).
[45] K. Binder and W. Paul, Macromolecules **41**, 4537 (2008).
[46] J. Ghosh and R. Faller, J. Chem. Phys. **128**, 124509 (2008).
[47] B. A. Patel, P. G. Debenedetti, and F. H. Stillinger, J. Phys. Chem. A **111**, 12651 (2007).
[48] F. A. Escobedo, J. Chem. Phys. **108**, 8761 (1998).
[49] A. L. Galbraith and C. Hall, Fluid Phase Equilib. **262**, 1 (2007).
[50] I. D. Gospodinov and F. A. Escobedo, J. Chem. Phys. **122**, 164103 (2005).
[51] B. A. Berg and T. Neuhaus, Phys. Lett. B **267**, 249 (1991).